

Ultra-high Compton Frequency, Parity Independent, Mesoscopic Schrödinger Cat Atom Interferometer with Heisenberg Limited Sensitivity

Resham Sarkar,^{1,*} Renpeng Fang,¹ and Selim M. Shahriar^{1,2}

¹*Department of Physics and Astronomy, Northwestern University, 2145 Sheridan Road, Evanston, IL 60208, USA*

²*Department of EECS, Northwestern University, 2145 Sheridan Road, Evanston, IL 60208, USA*

We present a protocol for an atomic interferometer that reaches the Heisenberg Limit (HL), via collective state detection and critical tuning of one axis twist spin squeezing. It generates a Schrödinger cat state, as a superposition of two collective states, and the interference occurs at an ultrahigh Compton frequency, reaching $\sim 2 \times 10^{31}$ Hz for a million ^{87}Rb atoms. The signal depends critically on the parity of atom number, N . It produces fringes narrowed by a factor of N for one parity, and zero signal for the other. It can be modified to reverse the roles of the two parities. Over repeated measurements under which the probability of being even or odd is equal, the signals from one parity get filtered out, and HL sensitivity is achieved for those corresponding to the other.

PACS numbers: 06.30.Gv, 03.75.Dg, 37.25.+k

The phase sensitivity of an atomic interferometer (AI) depends on the Compton frequency, $\omega_C = mc^2/\hbar$ of the individual particles interfering at non-relativistic velocities, where m is the mass of the particle, and c is the velocity of light in vacuum [1–4]. Matter wave interferometry with large molecules have successfully demonstrated the superposition of quantum states with large mass [5]. However, these interferometers, based on the Talbot effect, are not suited for rotation sensing, owing to constraints in fabricating gratings of small enough spacing, and associated effects of van der Waals interaction. An alternative approach is to make a large number (N) of particles, each with a mass m , behave as a single object with a mass of $M \equiv Nm$, and thus a Compton frequency of Mc^2/\hbar . In this letter, we describe a protocol that enables the realization of an atomic interferometer where two distinct quantum states of such a mesoscopic single object, each with this Compton frequency, are spatially separated and then recombined, leading to fringes that are a factor of N narrower than what is achieved with a conventional atomic interferometer. We show that the net metrological sensitivity of this interferometer is equivalent to the Heisenberg limited (HL) sensitivity of a conventional atomic interferometer. Aside from application to metrology, such a mesoscopic Schrödinger cat [6] interferometer may serve as a test-bed for the effect of gravitational interaction on macroscopic decoherence and quantum state reduction [7–11]. It also opens up a new regime for atom-interferometric measurement of gravitational red-shift [12] and for exploring performance of matter-wave clocks [13] in a regime with a much higher Compton frequency. We also show how such a mesoscopic single object can be used to increase the effective base frequency of an atomic clock by a factor of N , with a metrological sensitivity that is equivalent to the HL sensitivity of a conventional atomic clock.

Recently, we presented a Collective State Atomic Interferometer (COSAIN) [14], where we showed that the effect of large Compton frequency can be observed in

directly by detecting one of the collective states. These states, $\{|E_0\rangle, |E_1\rangle, \dots, |E_N\rangle\}$, commonly referred to as Dicke collective states, arise as a result of interaction of an ensemble of identical independent atoms with a semi-classical field [15–17]. The interferences between all of the collective states lead to a reduction in signal linewidth by a factor of \sqrt{N} as compared to a conventional Raman atomic interferometer (CRAIN). However, this reduction by a factor of \sqrt{N} in linewidth is countered by a corresponding reduction in the effective signal to noise ratio (SNR) since the system now behaves as a single particle. Therefore, the metrological sensitivity of a COSAIN is, under ideal conditions, the same as that of a CRAIN. A direct transition $|E_0\rangle \leftrightarrow |E_N\rangle$, bypassing all the intermediate collective states, would result in a signal of linewidth narrowed by a factor of N , thus yielding HL phase sensitivity despite the reduced SNR. However, there is no electric dipole coupling between $|E_0\rangle$ and $|E_N\rangle$ for non-interacting atoms, excluding the possibilities to achieve this goal with conventional excitation.

Here, we propose a new protocol that employs squeezing and a rotation, followed by another rotation and unsqueezing [18–20] in a COSAIN to attain the HL phase sensitivity. Explicitly, we apply one axis twist (OAT) spin squeezing [21–25] around the \hat{z} axis (defined as the spin-up direction) immediately following the first $\pi/2$ -pulse in a CRAIN, which aligns the mean spin vector along the \hat{y} axis. Prior to the application of the squeezing interaction, the population of the collective states follow a binomial distribution, corresponding to the Coherent Spin State (CSS) [16]. As the strength of squeezing is increased, the distribution begins to flatten out, eventually generating a Schrödinger cat state corresponding to an equal superposition of $|E_0\rangle$ and $|E_N\rangle$ [26] when the OAT is followed by a $\pi/2$ rotation around the \hat{x} axis. The usual dark- π -dark sequence follows, at the end of which we apply a corrective rotation by $\pi/2$ (rather than $-\pi/2$, due to the state inversion caused by the π -pulse) around the \hat{x} axis, and then apply a corrective reverse-OAT interaction

about the $\hat{\mathbf{z}}$ axis. Finally, the last $\pi/2$ pulse effectuates interference between the collective states and the signal is detected by measuring the population of one of the collective states. Since the process makes use of a superposition of two mesoscopic quantum states, we name this a Schrödinger Cat Atomic Interferometer (SCAIN).

In order to illustrate clearly the mechanism for realizing the SCAIN, and the characteristics thereof, as well as to establish the notations employed in the rest of this paper, it is useful to recall briefly the relevant features of a CRAIN and a COSAIN. A CRAIN makes use of N non-interacting identical three-level atoms with metastable hyperfine states $|\downarrow, p_z = 0\rangle$ and $|\uparrow, p_z = \hbar k\rangle$, (where $k = k_1 + k_2$, with k_1 and k_2 being the wave numbers for the two counter-propagating beams, and p_z being the z -component of the linear momentum), and an excited state $|e\rangle$, in the Λ -configuration, reduced to an equivalent two-level model [27]. We represent these atoms by a collective spin $\hat{\mathbf{J}} = \sum_i^N \hat{\mathbf{j}}_i$, where $\hat{\mathbf{j}}_i$ represents the pseudospin-1/2 operator for each atom. The ensemble is initially prepared in a Coherent Spin State (CSS), $|\mathbf{-\hat{z}}\rangle \equiv |E_0\rangle = \prod_{i=1}^N |\downarrow_i\rangle$. Here, we have employed the notation that $|\hat{\mathbf{w}}\rangle$ represents a CSS where the pseudo-spin of each atom is aligned in the direction of the unit vector $\hat{\mathbf{w}}$. Under a pulse sequence of $\pi/2$ –dark– π –dark– $\pi/2$, each atom's wavepacket first separates into two components, then gets redirected and finally recombined to produce an interference which is sensitive to any phase-difference, ϕ between the two paths. As an example, we consider the case of rotation where an AI gyroscope rotating at a rate Ω_G about an axis normal to the area Θ accrues a phase difference $\phi = 2\omega_C\Theta\Omega_G/c^2$ between its trajectories [28]. The effect of the overall phase shift ϕ due to rotation is uniformly spread throughout the interferometric sequence. However, for theoretical convenience, we introduce it in two equal parts during each of the dark zones (a rigorous justification of this approach can be found in Ref. [29]). The final state of the atoms is given by

$$|\psi\rangle = e^{-i\frac{\pi}{2}\hat{J}_x} e^{i\frac{\phi}{2}\hat{J}_z} e^{-i\pi\hat{J}_x} e^{-i\frac{\phi}{2}\hat{J}_z} e^{-i\frac{\pi}{2}\hat{J}_x} |\mathbf{-\hat{z}}\rangle = \prod_{i=1}^N -\frac{1}{2} e^{-i\phi/2} ((1 + e^{i\phi}) |\downarrow_i\rangle + i(1 - e^{i\phi}) |\uparrow_i\rangle). \quad (1)$$

In a CRAIN, ϕ is measured by mapping it onto the operator representing the difference in spin-up and spin-down populations: $\hat{J}_z = (\hat{N}_\uparrow - \hat{N}_\downarrow)/2$, where $\hat{N}_\uparrow = \sum_i |\uparrow_i\rangle\langle\uparrow_i|$ and $\hat{N}_\downarrow = \sum_i |\downarrow_i\rangle\langle\downarrow_i|$. The signal, which is a measure of the population of $|\downarrow\rangle$ is, therefore, $S_{CRAIN} = J + \langle -\hat{J}_z \rangle = N \cos^2(\phi/2)$, where $J = N/2$. The corresponding fringe linewidth is given by $\varrho = c^2/(2\omega_C\Theta)$. The measurement process causes wavefunction collapse of the individual spins from the superposition state to $|\downarrow\rangle$, resulting in quantum projection noise in the measure of the signal [30], $\Delta S_{CRAIN} =$

$\Delta(-\hat{J}_z) = \sqrt{N/4} \sin(\phi)$, where $\Delta\hat{J}_z$ is the standard deviation of \hat{J}_z . Assuming ideal quantum efficiency, the quantum fluctuation in rotation (QFR) is given by $\Delta\Omega_G|_{CRAIN} = |\Delta(-\hat{J}_z)/\partial\Omega_G(-\hat{J}_z)| = c^2/2\omega_C\Theta\sqrt{N}$, where $\partial\Omega_G \equiv \partial/\partial\Omega_G$.

The COSAIN differs from a CRAIN in that the measurement of the signal is done on a Dicke collective state of the ensemble, instead of a single atomic state [14]. The Dicke states are eigenstates of \hat{J}_z and can be represented as $|E_n, p_z = n\hbar k\rangle = \sum_{k=1}^{(N)} P_k |\downarrow^{N-n} \otimes \uparrow^n\rangle / \sqrt{\binom{N}{n}}$, where P_k is the permutation operator [15]. As a result of the first $\pi/2$ -pulse, the initial state $|E_0, p_z = 0\rangle$ is coupled to $|E_1, p_z = \hbar k\rangle$, which in turn is coupled to $|E_2, p_z = 2\hbar k\rangle$, and so on, all the way up to $|E_N, p_z = N\hbar k\rangle$. This causes the ensemble to split into $N + 1$ trajectories. The dark zone that immediately follows imparts a phase $e^{in\phi/2}$ to $|E_n\rangle$. At this point, the π -pulse generates a flip in the individual spins, causing $|E_n\rangle$ to become $|E_{N-n}\rangle$, and vice versa. The second dark-zone lends a phase $e^{i(0.5N-n)\phi}$ to $|E_n\rangle$. The mathematical derivation of this mechanism is discussed in detail in Ref. [14]. The last $\pi/2$ -pulse causes each of the collective states to interfere with the rest of the states. The COSAIN can, thus, be viewed as an aggregation of interference patterns due to $\binom{N+1}{2}$ interferometers working simultaneously. The narrowest constituent signal fringes are derived from interferences between states with the largest difference in phase, i.e. $|E_0\rangle$ and $|E_N\rangle$. The width of this fringe is ϱ/N . The widths of the rest of the signal components range from ϱ to $\varrho/(N-1)$. The signal, which is the measure of population of $|E_0\rangle$ is the result of the weighted sum of all the pairwise interferences with this state. This is detected by projecting the final state of the ensemble, $|\psi\rangle$ on $|E_0\rangle$. Thus, $S_{COSAIN} = \langle \hat{G} \rangle = \cos^{2N}(\phi/2)$, where $\hat{G} \equiv |E_0\rangle\langle E_0|$. The quantum projection noise is the standard deviation of \hat{G} , given by $\Delta S_{COSAIN} = \cos^N(\phi/2) \sqrt{1 - \cos^{2N}(\phi/2)}$. The QFR of the COSAIN is thus, $\Delta\Omega_G|_{COSAIN} = |\Delta\hat{G}/\partial\Omega_G\langle\hat{G}\rangle|$. Under quantum noise limited operation, this equals $(\Delta\Omega_G|_{CRAIN}/\sqrt{N}) |\sqrt{\sec^{4J}(\phi/2) - 1} / \tan(\phi/2)|$. Therefore, for $\Omega_G \rightarrow 0$, the rotation sensitivity of the COSAIN is same as that of a CRAIN, assuming all the other factors remain the same. One way of surpassing the SQL is to suppress the contribution of the constituent fringes broader than ϱ/N . This is precisely what happens in the SCAIN, which makes use of squeezed spin state (CSS) of the ensemble $|\psi_e\rangle = e^{-i\mu\hat{J}_z^2} |\hat{\mathbf{y}}\rangle$, where μ is the squeezing parameter, and $\hat{\mathbf{y}}$ is the quantum state produced by the first $\pi/2$ -pulse.

The SCAIN can be operated under two different protocols, which are essentially identical, except for the choice of the axis around which we apply the rotation that maximizes the degree of observed squeezing. In one case (Protocol A), the rotation is around the $\hat{\mathbf{x}}$ axis while in the other (Protocol B), the rotation is around the

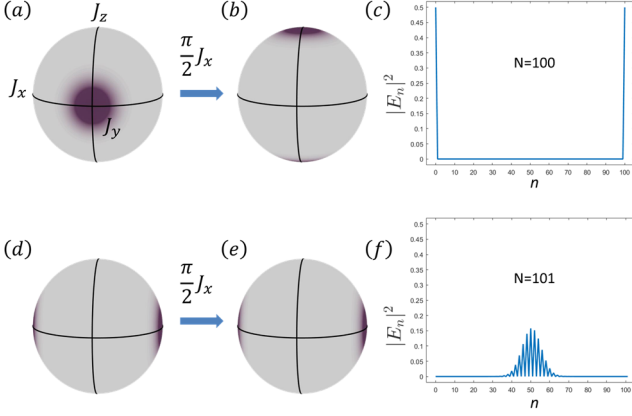


FIG. 1. Illustration of the SCAIN scheme for Protocol A. For even N : (a) For $\mu = \pi/2$, the Husimi quasi probability distribution (QPD) is split into two circular components located on the opposite faces normal to the $\hat{\mathbf{y}}$ axis of the Bloch sphere. (a→b) the QPD of the SSS state ($|\psi_e\rangle$) is rotated by $\pi/2$ about the $\hat{\mathbf{x}}$ axis to yield the Schrödinger cat state; note the components on both top and bottom of the Bloch sphere in (b). (c) Distribution of collective states in the rotated SSS, showing 50% in state $|E_0\rangle$ and 50% in state $|E_N\rangle$. For odd N : (d) For $\mu = \pi/2$, the QPD is split into two circular components located on the opposite faces normal to the $\hat{\mathbf{x}}$ axis of the Bloch sphere. (d→e) rotation about $\hat{\mathbf{x}}$ axis does not transform the SSS. (f) Distribution of collective states in the rotated SSS.

$\hat{\mathbf{y}}$ axis. We first consider Protocol A, focusing initially on the special case where the squeezing parameter μ is $\pi/2$, as illustrated in Fig. 1, with the case of an arbitrary value of μ to be discussed later. The OAT spin squeezing effect is achieved by applying the squeezing Hamiltonian, $H_{OAT} = \hbar\chi J_z^2$, for a duration of time τ such that $\mu = \chi\tau$. For even N , H_{OAT} transforms $|\hat{\mathbf{y}}\rangle$ to $|\psi_e\rangle = (|\hat{\mathbf{y}}\rangle - \eta|-\hat{\mathbf{y}}\rangle)/\sqrt{2}$, where $\eta = i(-1)^{N/2}$, representing a phase factor with unity amplitude. Rotating $|\psi_e\rangle$ by $\nu = \pi/2$ about the $\hat{\mathbf{x}}$ axis yields the Schrödinger cat state $|\psi_{SC}\rangle = (|E_0\rangle + \eta|E_N\rangle)/\sqrt{2}$. At the end of the intermediate dark– π –dark sequence, the state of the ensemble is $e^{i\phi J_z/2} e^{-i\pi J_x} e^{-i\phi J_z/2} |\psi_{SC}\rangle = (e^{iN\phi/2} \eta|E_N\rangle + e^{-iN\phi/2}|E_0\rangle)/\sqrt{2}$. As discussed above, the interference between states with a phase difference $N\phi$ produces signal fringes narrowed by a factor of N . To measure ϕ , we seek to undo the effect of squeezing on the system. This is accomplished in two steps. First, we apply another rotation $\nu = \pi/2$ (rather than $-\pi/2$, as noted earlier, due to the state inversion caused by the π -pulse) about the $\hat{\mathbf{x}}$ axis. Thereafter, the untwisting Hamiltonian, $-H_{OAT}$ is applied. Finally, the last $\pi/2$ pulse is applied to catalyze interference between the resulting states. The signal arising from this interference depends on ϕ as $S_{SC} = \langle \hat{G} \rangle = \sin^2(N\phi/2)$.

When N is odd, initial squeezing produces $|\psi_e\rangle = (|\hat{\mathbf{x}}\rangle + \zeta|-\hat{\mathbf{x}}\rangle)/\sqrt{2}$, where $\zeta = i(-1)^{(N+1)/2}$, representing a phase factor with unity amplitude. For $\phi = 0$, the

sequence $e^{-i\nu J_x} e^{i\phi J_z/2} e^{-i\pi J_x} e^{-i\phi J_z/2} e^{-i\nu J_x}$ only causes an identical phase change in each of these states. Application of the unsqueezing Hamiltonian, $-H_{OAT}$ then restores the system to $|\hat{\mathbf{y}}\rangle$, and the final $\pi/2$ pulse places the system in the $|\hat{\mathbf{z}}\rangle$ state, which is the same as the collective state $|E_N\rangle$. Since we detect the collective state $|E_0\rangle$, the whole sequence thus generates a null signal. For reasons that are not manifestly obvious due to the complexity of the states, but can be verified via simulation, the same conclusion holds for an arbitrary value of ϕ . Over repeated measurements, the probability of N being even or odd is equal. Thus, for M trials, the average signal of the SCAIN in this regime is $S_{SC} = M \sin^2(N\phi/2)/2$. The associated quantum projection noise is $\Delta S_{SC} = \sqrt{M/2} \sin(N\phi)$. The QFR is thus, $\Delta\Omega_G = c^2/\sqrt{2MN\omega_C\Theta}$. It should be noted that the phase factors η and ζ depend, respectively, on the super even parity (SEP), representing whether $N/2$ is even or odd, and the super odd parity (SOP), representing whether $(N+1)/2$ is even or odd. However, in each case, the shapes of the fringes as well as the values of QFR, are not expected to depend on the value of SEP and SOP, as we have verified explicitly.

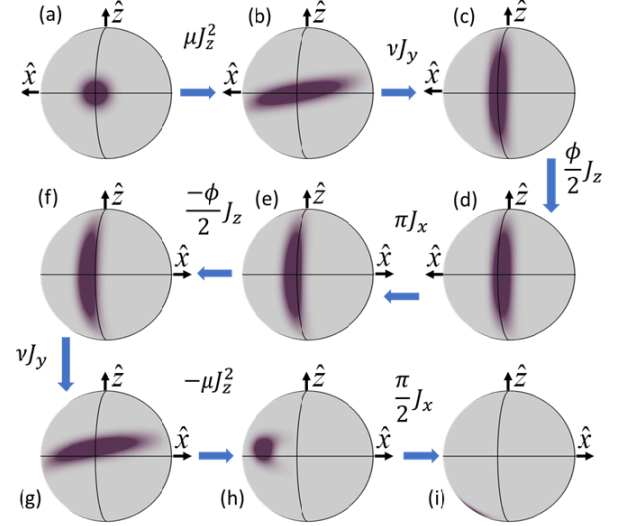


FIG. 2. Illustration of the SCAIN scheme for Protocol B. The Husimi quasiprobability distribution of state evolution for $\mu < \pi/2$: The initial CSS $|\hat{\mathbf{y}}\rangle$ (a) evolves under H_{OAT} to (b) which is then rotated by an angle ν (b→c) so as to maximize the fluctuations along $\hat{\mathbf{z}}$. (d) The first dark zone imparts a phase $\phi/2$. (e) The Bloch sphere is rotated to show the other face where the SSS is situated after the π pulse. (f) The second dark zone imparts an additional $\phi/2$ phase. (d→g) The spins are unrotated by the same angle ν and then (h) unsqueezed, by applying the inverse of H_{OAT} . (i) The final $\pi/2$ pulse causes interference between the two paths of the interferometer.

Next, we consider Protocol B, as illustrated in Fig. 2. Following the application of the squeezing interaction, the rotation axis and ν are chosen so as to maximize

(at this stage of the process) the fluctuations along $\hat{\mathbf{z}}$. This is achieved by rotating the SSS about the direction of the mean spin vector, $\hat{\mathbf{y}}$. Prior to rotation, the SSS has the same binomial distribution of collective states as the original CSS, although with different relative phases among them. The rotation causes a reshuffle in the population of the collective states, and the distribution begins to flatten out. For a given value of N , ν increases with μ , reaching maximum value of $\pi/2$ at $\mu = \mu_0$ (a typical value of μ_0 is 0.05 for $N = 100$, for example). For a large ensemble, μ_0 can be achieved for a very short evolution time. When squeezed beyond μ_0 , the distribution begins to invert, and the relative proportion of the extremal states increases. The exact state distribution is determined by whether N is even or odd. At $\mu = \pi/4$, the QPD splits into four identical parts. The distribution of collective state populations is trimodal for even N , and bimodal for odd N . The distribution of collective state populations for various values of μ can be seen in Figure 1 of the Supplement.

Once the SSS is optimally aligned, the usual dark– π –dark sequence follows. We first apply another rotation ν about $\hat{\mathbf{y}}$ axis, and then apply $-H_{OAT}$. Finally, the last $\pi/2$ pulse is applied to catalyze interference between the two paths of the interferometer. For $\phi = 0$, the original CSS is restored. However, for $\phi \neq 0$, the final state is shifted along J_x . Until the value of μ gets close to $\pi/2$, the central fringe as a function of ϕ is essentially identical for both odd and even values of N . Thus, for M trials, the average signal is independent of the parity of N for the central fringe, which is the only one relevant for metrological applications. For different values of μ , the non-central fringes, averaged over the odd and even cases, have different shapes, heights and widths. However, the central fringe always has full visibility. Due to non-binomial distribution of the collective states, the width of the central fringe is significantly narrower than that in the corresponding COSAIN with the same number of atoms. The width of the central fringe first decreases sharply with increasing values of μ , and then saturates at $\mu = \mu_0$. Consequently, the fluctuations in rotation sensitivity plummets, attaining the minimum value $\Delta\Omega_G|_{SCAIN} = e^{1/3}c^2/2\sqrt{MN}\omega_C\Theta$, at $\mu = \mu_0$. This process is illustrated in Fig. 3 (a)–(e), for various values of μ . The results for even values of N ($N = 200$) are indicated by the red lines, and those for the odd values of N ($N = 201$) are indicated by the blue (dashed or dotted) lines. In Fig. 3 (f), we show the corresponding fringes produced using Protocol A, for the special case of $\mu = \pi/2$. As described earlier, in this case, we get a purely sinusoidal fringe pattern for even values of N , and a null signal for odd values of N . The averaged signal, therefore, is also purely sinusoidal. The width of these fringes is a factor of N narrower than what is observed in a CRAIN.

For the limiting case of $\mu = \pi/2$, Protocol B pro-

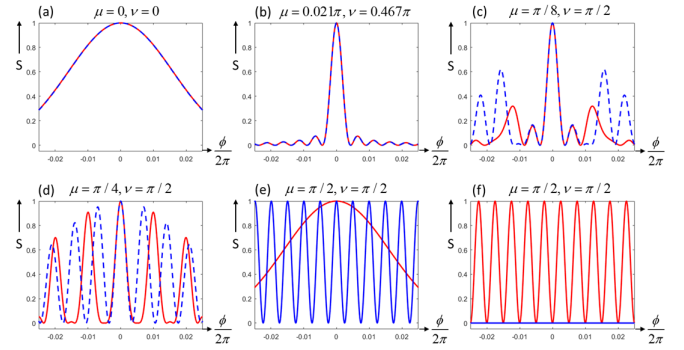


FIG. 3. Signal fringes for various values of μ . $N = 200$ is indicated by red lines, $N = 201$ by blue (dashed or solid) lines. Figures (a)–(e) employ Protocol B, while figure (f) employs Protocol A. The phase span is $1/20$ -th of 2π ; as such, we see 10 red fringes in figure (f), thus demonstrating a factor of N reduction in the width of fringes for Protocol A.

duces very different results for odd and even values of N . Specifically, for odd values of N , this protocol produces uniform fringes, each with a width that is factor of N narrower than what is observed in a CRAIN, thus yielding HL sensitivity. In this case, the ideal Schrödinger Cat state is realized, in a manner analogous to what we described above for Protocol A (with $\mu = \pi/2$). For odd values of N , this protocol also produces uniform fringes, but each with a width that is the same as that observed for COSAIN (which is a factor of \sqrt{N} narrower than what is observed in a CRAIN), thus yielding SQL sensitivity. The average of these two signals, for many repeated measurements, would produce a sensitivity that, for large N , is lower than the HL by a factor of $\sqrt{2}$ [29]. In addition, due to the mixing of the suboptimal signal contributed by the instances corresponding to even values of N , Protocol B, even for $\mu = \pi/2$, is not well-suited for experiments aimed at studying the effects of gravity on clear superposition of just two macroscopic states [7–10], measuring gravitational red-shift [12], and realizing a matter-wave clock with very high Compton frequency [13].

In Fig. 4, we summarize the results for both protocols, for squeezing parameters ranging from $\mu = 0$ to $\mu = \pi/2$. Here, we show the inverse of the QFR, normalized to the same for the HL for $N = 100$, as a function of μ . Horizontal lines indicate the HL (black solid), and the SQL (black dashed). The dotted blue lines corresponds to odd value of N ($N = 101$) and the red lines corresponds to even value of N ($N = 100$). The left panel shows the result of using Protocol B. The value of QFR^{-1} increases monotonically, reaching a peak value at $\mu = \mu_0$, and then remains flat until getting close to $\mu = \pi/2$, with virtually no difference between the odd and even values of N , as discussed in detail earlier. Near $\mu = \pi/2$, the value of QFR^{-1} begins to diverge, reaching the HL(SQL) for odd(even) values of N at $\mu = \pi/2$. The right panel shows the result of using Protocol A. At $\mu = \pi/2$, QFR^{-1}

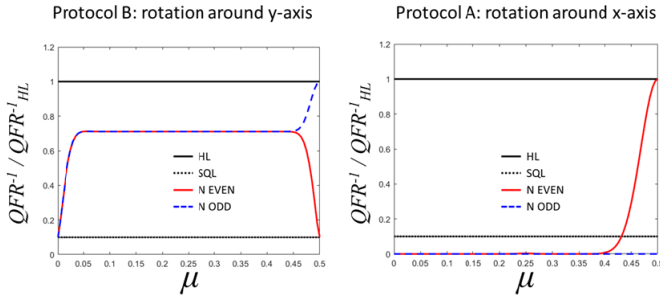


FIG. 4. QFR^{-1} of SCAIN as a function of the squeezing parameter, μ , normalized to the HL for $N = 100$. Horizontal lines indicate the HL (black solid) and the SQL (black dashed). The dashed blue lines correspond to odd value of N ($N = 101$) and the red lines correspond to even value of N ($N = 100$). The left(right) panel shows the results for Protocol B(A).

is at the HL for even values of N , and vanishes for odd values of N . For $\mu < \pi/2$, the amplitude of the signal for even values of N decreases rapidly, with corresponding decrease in the value of QFR^{-1} . It should be noted that a vanishing value of QFR^{-1} is due simply to the vanishing of the signal itself.

Finally, we note that a similar treatment of the Collective State Atomic Clock [31] also produces similar results. Such a clock can be called a SCAC (Schrödinger Cat Atomic Clock). In this case, the Schrödinger Cat state corresponds to a situation where the effective base frequency of the clock is increased by a factor of N . Again, if we consider only the case of even number of atoms, the SCAC reaches the HL sensitivity. If the cases of odd number of atoms are also taken into account, then the sensitivity is within a factor of $\sqrt{2}$ of the HL. The details of the SCAC are shown in the Supplement [32].

This work has been supported by the NSF grants number DGE-0801685 and DMR-1121262, and AFOSR grant number FA9550-09-01-0652.

also be derived using de Broglie wavelength. However, it can be shown that this approach simply corresponds to interference at the Compton frequency in a moving frame, as shown in Ref. [13, 14].

- [5] S. Eibenberger, S. Gerlich, M. Arndt, M. Mayor, and J. Tüxen, *Phys. Chem. Chem. Phys.* 15, 14696 (2013).
- [6] E. Schrödinger, *Naturwissenschaften* 23, 807(1935); English translation by J. D. Trimmer, *Proc. Am. Philos. Soc.* 124, 323 (1980).
- [7] L. Diosi, *Phys. Rev. A* 40, 1165–1174 (1989).
- [8] R. Penrose, *Gen. Relativ. Gravit.* 28, 581–600 (1996).
- [9] W. Marshall, C. Simon, R. Penrose, and D. Bouwmeester, *Phys. Rev. Lett.* 91(13–16), 130401 (2003).
- [10] R. Penrose, *Foundations of Physics*, 44: 557–575 (2014)
- [11] I. Pikovski, M. Zych, F. Costa, Č. Brukner, *Nature Physics* 11, 668–672 (2015).
- [12] H. Müller, A. Peters, and S. Chu, *Nature* 463, 926–929 (2010).
- [13] S.-Y. Lan et al., *Science* 339, 554–557 (2013).
- [14] R. Sarkar, M. E. Kim, R. Fang, S. M. Shahriar, *Phys. Rev. A* 92 (6), 063612.
- [15] R. Sarkar, M. E. Kim, R. Fang, Y. Tu, and S. M. Shahriar, *J. Mod. Opt.* **62**, 1253 (2015).
- [16] F. T. Arecchi, E. Courtens, R. Gilmore and H. Thomas, *Phys. Rev. A* 6, 2211 (1972).
- [17] R. H. Dicke, *Phys. Rev.* 93, 99 (1954).
- [18] B. Yurke, S. L. McCall, and J. R. Klauder, *Phys. Rev. A* 33, 4033 (1986).
- [19] F. Toscano, D. A. R. Dalvit, L. Davidovich, and W. H. Zurek, *Phys. Rev. A* 73, 023803 (2006).
- [20] G. Goldstein, P. Cappellaro, J. R. Maze, J. S. Hodges, L. Jiang, A. S. Sørensen, and M. D. Lukin, *Phys. Rev. Lett.* 106, 140502 (2011).
- [21] M. Kitagawa, M. Ueda, *Phys. Rev. A* 47, 5138.
- [22] M. H. Schleier-Smith, I. D. Leroux, and V. Vuletic, *Phys. Rev. A* 81, 021804 (2010).
- [23] I. D. Leroux, M. H. Schleier-Smith, and V. Vuletic, *Phys. Rev. Lett.* 104, 073602 (2010).
- [24] Y.-L. Zhang, C.-L. Zou, X.-B. Zou, L. Jiang, and G.-C. Guo, *Phys. Rev. A* 91, 033625 (2015).
- [25] A. Søndberg Sørensen and K. Mølmer, *Phys. Rev. A* 66, 022314 (2002).
- [26] K. Mølmer and A. S. Sørensen, *Phys. Rev. Lett.* 82, 1835 (1999).
- [27] M. S. Shahriar, M. Jheeta, Y. Tan, P. Pradhan, and A. Gangat, *Opt. Comm.* 243, 183 (2004).
- [28] E. J. Post, *Rev. of Mod. Phys.* 39, no. 2 (1967).
- [29] R. Fang, R. Sarkar, and S. M. Shahriar, <https://arxiv.org/pdf/1707.08260.pdf> (2017)
- [30] W. M. Itano, J. C. Bergquist, J. J. Bollinger, J. M. Gilligan, D. J. Heinzen, F. L. Moore, M. G. Raizen, and D. J. Wineland, *Phys. Rev. A* **47**, 3554–3570 (1993).
- [31] M. E. Kim, R. Sarkar, R. Fang, S. M. Shahriar, *Phys. Rev. A* 91, (6), 063629.
- [32] Supplementary material

* rsarkar@u.northwestern.edu

- [1] C.J. Bordé, *Phys. Lett. A* 140 (1989) 10.
- [2] M. Kasevich, S. Chu, *Phys. Rev. Lett.* 67 (1991) 181.
- [3] F. Riehle, Th. Kisters, A. Witte, J. Helmcke, and Ch. J. Bordé, *Phys. Rev. Lett.* 67, 177 (1991).
- [4] The signal corresponding to an atomic interferometer can

Ultra-high Compton Frequency, Parity Independent, Mesoscopic Schrödinger Cat Atom Interferometer with Heisenberg Limited Sensitivity

Supplementary Material

Resham Sarkar,^{1,*} Renpeng Fang,¹ and Selim M. Shahriar^{1,2}

¹*Department of Physics and Astronomy, Northwestern University, 2145 Sheridan Road, Evanston, IL 60208, USA*

²*Department of EECS, Northwestern University,*

2145 Sheridan Road, Evanston, IL 60208, USA

SCHRÖDINGER CAT ATOMIC CLOCK

As mentioned in the main body of the paper, the combination of one axis twist (OAT) spin squeezing, followed by a rotation, inversion of rotation and unsqueezing, along with collective state detection can also be used to realize a parity-independent, mesoscopic Schrödinger Cat Atomic Clock (SCAC) with Heisenberg Limited sensitivity. In order to describe how the SCAC works, we consider first a configuration where the ground states $|\downarrow\rangle$ and $|\uparrow\rangle$ of a three-level atom interact with an excited state $|e\rangle$ via two copropagating laser beams. One of the beams, detuned from resonance by δ_1 and with Rabi frequency Ω_1 , couples $|\downarrow\rangle$ to $|e\rangle$. The other beam, with Rabi frequency Ω_2 and detuning δ_2 , couples $|e\rangle$ to $|\uparrow\rangle$. For $\delta \gg \Omega_1, \Omega_2, \Gamma$, where $\delta = (\delta_1 + \delta_2)/2$, and Γ is the decay rate of $|e\rangle$, the interaction can be described as an effective two level system excited by an effective traveling wave with a Rabi frequency $\Omega = \Omega_1\Omega_2/2\delta$, and detuning $\Delta = \delta_1 - \delta_2$. It should be noted that this is formally equivalent to a conventional microwave atomic clock that couples $|\downarrow\rangle$ to $|\uparrow\rangle$. However, since a Raman transition is needed for the detection of collective states, we choose to describe it here as a Raman clock. In practice, all results presented here would remain valid for a conventional microwave excitation, which is preferable because a Raman clock may suffer from fluctuations in light shifts.

In a conventional Raman Ramsey atomic clock (RRAC), an ensemble of N effective two-level atoms is first prepared in the CSS, denoted as $|-z\rangle \equiv |E_0\rangle = \prod_{i=1}^N |\downarrow_i\rangle$. The initial $\pi/2$ -pulse rotates the CSS about the \hat{x} -axis and brings it to the \hat{y} -axis, producing the state $e^{-i(\pi/2)J_x} |-z\rangle = |\hat{y}\rangle = \prod_{i=1}^N (|\downarrow_i\rangle - i|\uparrow_i\rangle)/\sqrt{2}$. The collective spin is then left to evolve without any interaction for time T_D , during which each constituent spin acquires a phase $\phi = 2\pi f T_D$, where $f = \Delta/2\pi$ is the (two-photon) detuning of the clock in Hertz. This is equivalent to a rotation by ϕ about the \mathbf{z} -axis. At this point, a second $\pi/2$ -pulse is applied, which establishes the final state, $|\psi\rangle = \prod_{i=1}^N ((1 - e^{i\phi})|\downarrow\rangle - i(1 + e^{i\phi})|\uparrow\rangle)/2$. The aim of the RRAC is to measure ϕ , and therefore, f as precisely as possible.

In an ideal RRAC, ϕ is measured by mapping it onto the operator representing the difference in spin-up and spindown populations: \hat{J}_z . The signal, which is a mea-

sure of the population of $|\uparrow\rangle$ is, therefore, $S_{RRAC} = J + \langle \hat{J}_z \rangle = N \cos^2(\phi/2)$. The associated quantum projection noise is $\Delta S_{RRAC} = \Delta \hat{J}_z = \sqrt{N/4} \sin(\phi)$. The stability of the measurement of f is an indicator of the performance of an atomic clock. The stability of the clock is attributed to the quantum fluctuation in frequency (QFF), analogous to the QFR described in the main body of this paper. The QFF can be written as

$$QFF = \Delta f = \left| \frac{\Delta J_z}{\partial \langle J_z \rangle / \partial f} \right| = \left(2\pi T_D \sqrt{N} \right)^{-1} \equiv \gamma / \sqrt{N}. \quad (1)$$

where γ is the width of the RRAC fringes. As is the case for a COSAIN, the COSAC differs from a conventional RRAC in that the measurement of the signal is done on a collective state of the ensemble, instead of single atom measurements [1]. The first $\pi/2$ -pulse couples the initial state $|E_0\rangle$ to $|E_1\rangle$, which in turn is coupled to $|E_2\rangle$, and so on, effectively causing the ensemble to split into $N+1$ states. During the dark zone, the n -th collective state $|E_n\rangle$ picks up a phase $e^{-in\phi}$. When the ensemble interacts with the last $\pi/2$ -pulse, each of the collective states interfere with the rest of the states. The COSAC can, thus, be viewed as the aggregation of interference patterns due to $\binom{N+1}{2}$ RRAC's working simultaneously. The mathematical derivation of this mechanism is discussed in detail in Ref [1]. The narrowest constituent signal fringes are derived from interferences between states with the largest difference in phase, i.e. $|E_0\rangle$ and $|E_N\rangle$. The width of this fringe is γ/N . The widths of the rest of the signal components range from γ to $\gamma/(N-1)$. The signal, which is the measure of population of $|E_N\rangle$ is the result of the weighted sum of all the pairwise interferences with this state. This is detected by projecting the final state of the ensemble, $|\psi\rangle$ on $|E_N\rangle$. Thus, $S_{COSAC} = \langle \hat{Q} \rangle = \cos^{2N}(\phi/2)$, where $\hat{Q} \equiv |E_N\rangle \langle E_N|$. The quantum projection noise is the standard deviation of \hat{Q} , given by $\Delta S_{COSAC} = \cos^N(\phi/2) \sqrt{1 - \cos^{2N}(\phi/2)}$. The QFF of the COSAC is thus,

$$\Delta f|_{COSAC} = \left| \Delta \hat{Q} / \partial_f \langle \hat{Q} \rangle \right| = (\Delta f|_{CRAIN} / \sqrt{N}) \sqrt{\sec^4(\phi/2) - 1 / \tan(\phi/2)} \quad (2)$$

Therefore, for $f \rightarrow 0$, the frequency sensitivity of the COSAC is the same as that of an RRAC, assuming that all the other factors remain the same.

The Schrödinger Cat Atomic Clock (SCAC) is based on the same process of squeezing followed by a rotation and then another rotation and unsqueezing as that employed for the SCAIN. The CSS after the first $\pi/2$ -pulse is squeezed via the OAT spin squeezing Hamiltonian, $H_{OAT} = \hbar\chi J_z^2$, yielding the squeezed spin state (SSS) of the ensemble $|\psi_e\rangle = e^{-i\mu J_z^2} |\hat{\mathbf{y}}\rangle$, where $\mu = \chi\tau$ is the squeezing parameter, and τ is the duration of the squeezing interaction. This SSS must be rotated by an angle ν about an appropriate axis, the choice of which depends on the degree of squeezing, and follows the same rules as described in the main body of the paper.

Similar to the SCAIN, the SCAC can be operated under two different protocols, which are essentially identical, except for the choice of the axis around which we apply a rotation that maximizes the degree of observed squeezing, and the amount of the rotation. In one case (Protocol A), the rotation is around the $\hat{\mathbf{x}}$ axis, and the amount of rotation is always $\pi/2$. In the other case (Protocol B), the rotation is around the $\hat{\mathbf{y}}$ axis, and the amount of rotation depends on the degree of squeezing. We first consider Protocol A, focusing initially on the special case where $\mu = \pi/2$, with the case of an arbitrary value of μ to be discussed later. For even N , H_{OAT} transforms $|\hat{\mathbf{y}}\rangle$ to $|\psi_e\rangle = (|\hat{\mathbf{y}}\rangle - \eta|-\hat{\mathbf{y}}\rangle)/\sqrt{2}$, where $\eta = i(-1)^{N/2}$, representing a phase factor with unity amplitude. As we noted in the main body of this paper, this phase factor depends on the SEP; however, the shapes of the fringes, as well as the values of QFF, are not expected to depend on the value of the SEP, as we have verified explicitly. Rotating $|\psi_e\rangle$ by $\nu = \pi/2$ about the $\hat{\mathbf{x}}$ axis yields the Schrödinger cat state $|\psi_{SC}\rangle = (|E_0\rangle + \eta|E_N\rangle)/\sqrt{2}$. At the end of the dark zone, the state of the ensemble is $(e^{iN\phi/2}\eta|E_N\rangle + e^{-iN\phi/2}|E_0\rangle)/\sqrt{2}$. We now apply a rotation of $\nu = \pi/2$ about the $\hat{\mathbf{x}}$ axis (Ideally inversion of the rotation could require the application of rotation of $\nu = -\pi/2$). However, we have found [2] that changing the sign of this rotation simply inverts the final fringes. This is also true for the SCAIN protocol. It should also be noted that experimentally, $\nu = -\pi/2$ actually corresponds to $\nu = 3\pi/2$, which requires a longer duration or more power. Therefore, for both the SCAIN and the SCAC, we choose to use a corrective rotation of $\pi/2$ rather than $-\pi/2$, followed by the untwisting Hamiltonian, $-H_{OAT}$. Finally, the last $\pi/2$ pulse is applied to catalyze interference between the resulting states. The signal arising from this interference depends on ϕ as $S_{SCAC} = \langle \hat{Q} \rangle = \sin^2(N\phi/2)$.

When N is odd, initial squeezing produces $|\psi_e\rangle = (|\hat{\mathbf{x}}\rangle + \rho|-\hat{\mathbf{x}}\rangle)/\sqrt{2}$, where $\rho = i(-1)^{(N+1)/2}$, representing a phase factor with unity amplitude. As noted in the main body of the paper, this phase factor depends on the SOP; however, the shapes of the fringes, as well as the

values of QFF, are not expected to depend on the value of the SOP, as we have verified explicitly. For $\phi = 0$, the sequence $e^{-i\nu J_x} e^{-i\phi J_z} e^{-i\nu J_x}$ causes a π phase-shift in each of the components of this state. Application of the unsqueezing Hamiltonian, $-H_{OAT}$ then moves the system to $|-\hat{\mathbf{y}}\rangle$, and the final $\pi/2$ pulse places the system in the $|-\hat{\mathbf{z}}\rangle$ state, which is the same as the collective state $|E_0\rangle$. Since we detect the collective state $|E_N\rangle$, the whole sequence thus generates a null signal. Again, just as in the case of the SCAIN, same conclusion holds for an arbitrary value of ϕ , for reasons that are not manifestly obvious due to the complexity of the states, but can be verified via simulation. Over repeated measurements, the probability of N being even or odd is equal. Thus, for M trials, the average signal of the SCAC in this regime is $S_{SCAC} = M \sin^2(N\phi/2)/2$. The associated quantum projection noise is $\Delta S_{SCAC} = \sqrt{M/2} \sin(N\phi)$. The QFF is thus, $\Delta f = 1/\sqrt{2M\pi N T_D}$.

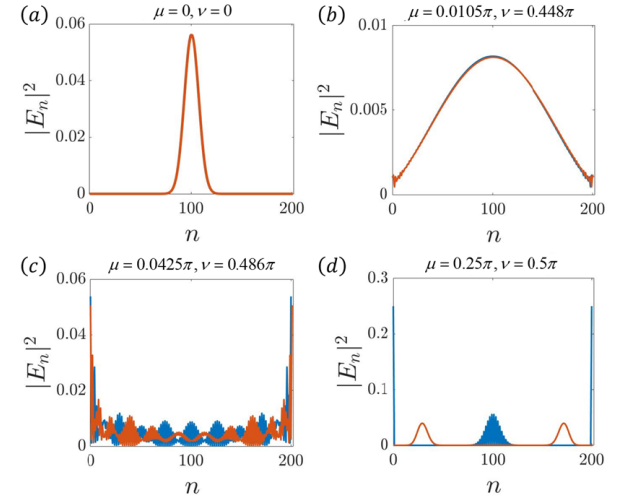


FIG. 1. Variation of population of collective states for different values of μ , under Protocol B. Both even (blue line) and odd (red line) values of N are considered. These results hold for both SCAIN and SCAC.

Next, we consider Protocol B. The rotation axis and the rotation angle ν are chosen so as to maximize the fluctuations along $\hat{\mathbf{z}}$ (at this point of the protocol). This is achieved by rotating the SSS about the direction of the mean spin vector, $\hat{\mathbf{y}}$. Prior to rotation, the SSS has the same binomial distribution of the collective states as in the original CSS, as depicted in Fig 1(a). The rotation causes a reshuffle in the population of the collective states, and the distribution begins to flatten out (Fig 1(b)). For a given value of N , ν increases with μ , reaching maximum value of $\pi/2$ at $\mu = \mu_0$. When squeezed beyond μ_0 , the distribution begins to invert, and the relative proportion of the extremal states increases. The exact state distribution is determined by whether N is even or odd (Fig 1(c)). At $\mu = \pi/4$, the QPD splits into four identical parts. For even N , the

distribution of collective state populations is trimodal, as depicted by the blue line in Fig. 1(d). On the other hand, for odd N , the distribution of collective state populations is bimodal, as shown in Fig. 1(d) (red line).

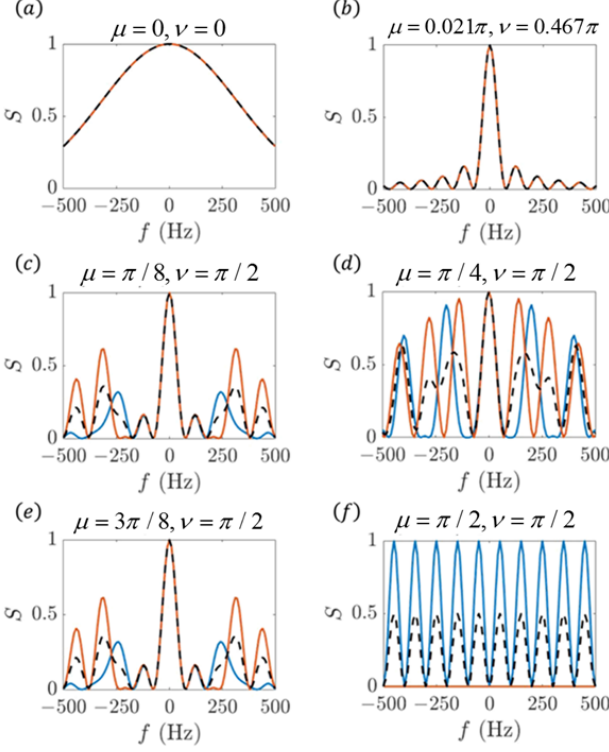


FIG. 2. Signal fringes for various values of μ , $T_D = 50 \mu\text{s}$. $N = 200$ is indicated by blue lines, $N = 201$ by red lines. The broken black lines indicate the average signal. Figures (a)-(e) employ Protocol B, while figure (f) employs Protocol A. The time interval between the $\pi/2$ pulses is $50 \mu\text{s}$, so that the peak-to-peak width of a conventional clock fringe would be 20 kHz . The peak-to-peak width of the blue fringes in figure (f) is seen to be 100 kHz , corresponding to a factor of N reduction for Protocol A.

Once the SSS is optimally aligned, the dark zone follows. We now apply another rotation $-\nu$ about \hat{y} axis (note that this rotation is a reversal of the original rotation, unlike the case for Protocol B in SCAIN), then apply $-H_{OAT}$. Finally, the last $\pi/2$ pulse is applied to catalyze interference between each of the resulting states. For $\phi = 0$, the original CSS is restored. However, for $\phi \neq 0$, the final state is shifted along J_x . Until the value of μ gets close to $\pi/2$, the central fringe as a function of frequency is essentially identical for both odd and even values of N . Thus, for M trials, the average signal is independent of the parity of N for the central fringe, which is the only one relevant for metrological applications. For different values of μ , the non-central fringes, averaged over the odd and even cases, have different shapes, heights and widths. However, the central fringe always has full visibility. Due to non-binomial distribution of the

collective states, the width of the central fringe is significantly narrower than that in the corresponding COSAC with the same number of atoms. The width of the central fringe first decreases sharply with increasing values of μ , and then saturates at $\mu = \mu_0$. Consequently, the fluctuations in frequency drops significantly, attaining the minimum value $\Delta f|_{SCAC} = e^{1/3}/\sqrt{M}2\pi NT_D$, at $\mu = \mu_0$.

This process is illustrated in Fig. 2 (a)-(e), for various values of μ . The results for even values of N ($N = 200$) are indicated by the blue lines, and those for the odd values of N ($N = 201$) are indicated by the orange lines. The broken black lines indicate the average signal. In Fig. 2 (f), we show the corresponding fringes produced using Protocol A, for the special case of $\mu = \pi/2$. As described earlier, in this case, we get a purely sinusoidal fringe pattern for even values of N , and a null signal for odd values of N . The averaged signal, therefore, is also purely sinusoidal. The width of these fringes is a factor of N narrower than what is observed in an conventional Raman Ramsey Atomic Clock (RRAC).

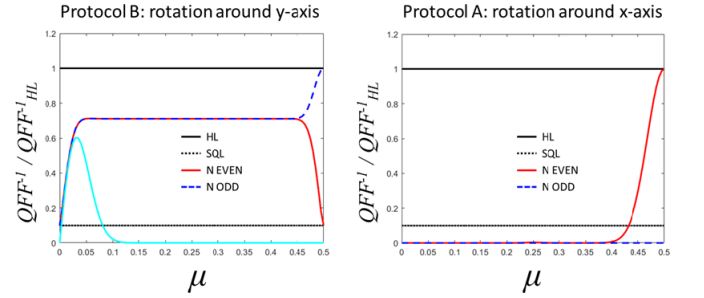


FIG. 3. QFF^{-1} of SCAC vs the squeezing parameter, μ , normalized by the same for the HL for $N = 100$. Horizontal lines indicate the HL (black solid), and the SQL (black dashed). The dashed blue lines corresponds to odd value of N ($N = 101$) and the red lines corresponds to even value of N ($N = 100$). The left(right) panel shows the results for Protocol B(A). The cyan line in the left panel shows the corresponding result for the squeezing-unsqueezing protocol proposed in Ref. [3] and demonstrated subsequently in Ref. [4].

For the limiting case of $\mu = \pi/2$, Protocol B produces very different results for odd and even values of N . Specifically, for odd values of N , this protocol produces uniform fringes, each with a width that is factor of N narrower than what is observed in an RRAC, thus yielding HL sensitivity. In this case, the ideal Schrödinger Cat state is realized, in a manner analogous to what we described above for Protocol A (with $\mu = \pi/2$). For odd values of N , this protocol also produces uniform fringes, but each with a width that is the same as that observed for COSAC (which is a factor of \sqrt{N} narrower than what is observed in an RRAC), thus yielding SQL sensitivity. The average of these two signals, for many repeated measurements, would produce a sensitivity that, for large N , is lower than the HL by a factor of $\sqrt{2}$ [2].

In Fig. 3, we summarize the results for both proto-

cols, for squeezing parameters ranging from $\mu = 0$ to $\mu = \pi/2$. The behavior is essentially identical to that shown in Figure 4 in the main body of the paper for the SCAIN. Here, we show the inverse of the QFF, normalized to the same for the HL for $N = 100$, as a function of μ . Horizontal lines indicate the HL (black solid), and the SQL (black dashed). The blue lines corresponds to odd value of N ($N = 101$) and the red lines corresponds to even value of N ($N = 100$). The left panel shows the result of using Protocol B. The value of QFF^{-1} increases monotonically, reaching a peak value at $\mu = \mu_0$, and then remains flat until getting close to $\mu = \pi/2$, with virtually no difference between the odd and even values of N . Near $\mu = \pi/2$, the value of QFF^{-1} begins to diverge, reaching the HL (SQL) for odd (even) values of N at $\mu = \pi/2$. The cyan line in the left panel shows, for comparison, the corresponding behavior of the squeezing-unsqueezing (SU) protocol recently proposed in Ref. [3] and demonstrated subsequently in Ref. [4]. This protocol also produces a sensitivity close to the HL, but only for a particular value of μ , and then drops off rapidly for both decreasing and increasing values of μ . In contrast, the Protocol B pro-

posed here reaches a sensitivity that is slightly higher than that attainable for the SU protocol, and is highly insensitive to the precise value of μ after reaching the plateau, as shown in the left panel of Fig. 3. The right panel shows the result of using Protocol A. At $\mu = \pi/2$, QFF^{-1} is at the HL for even values of N , and vanishes for even values of N . For $\mu < \pi/2$, the amplitude of the signal for even values of N decreases rapidly, with corresponding decrease in the value of QFF^{-1} . Just as in the case of the SCAIN, the vanishing value of QFF^{-1} is due simply to the vanishing of the signal itself.

* rsarkar@u.northwestern.edu

- [1] M. E. Kim, R. Sarkar, R. Fang, S. M. Shahriar, Phys. Rev. A 91, (6), 063629.
- [2] S. M. Shahriar, R. Fang, and R. Sarkar, <https://arxiv.org/pdf/1707.08260.pdf> (2017)
- [3] E. Davis, G. Bentsen, and M. Schleier-Smith, Phys. Rev. Letts. 116, 053601 (2016)
- [4] O. Hosten, R. Krishnakumar, N. J. Engelsen and M. A. Kasevich, Science 352, 1552 (2016)